SOL modelling of the JT-60SA tokamak initial operational scenario using SOLEDGE-EIRENE code

K. Gałązka[1]*, L. Balbinot[2], G. L. Falchetto[1], N. Rivals[1], P. Tamain[1], Y. Marandet[3], H. Bufferand[1], P. Innocente[2] and G. Ciraolo[1]

[1] *CEA, IRFM, F-13108 Saint-Paul-Lez-Durance, France*

[2] *Consorzio RFX, Corso Stati Uniti 4, 35127 Padova, Italy*

[3] *Aix-Marseille Univ., CNRS, PIIM, Marseille, France*

The main aim of this work is to assess the realistic heat loads on the first wall of the JT-60SA vessel. To achieve this scope, for the first time the entire vessel and the subdivertor region is modeled by the fluid transport code SOLEDGE-EIRENE [1]. Whereas the nominal scenario modeling was reported elsewhere [2] here we focus on the initial phase of scenario #2 with carbon divertor and limited heating power.

Simulation setup SOLEDGE-EIRENE is used in transport mode for the full current inductive scenario #2 of JT-60SA with the following setup: plasma influx at core boundary $S_i = 1 \cdot 10^{21}$ part./s, auxiliary heating power at core boundary within the interval $P_{aux} = [15, 30]$ MW with 2.5 MW steps, divided 50/50 between ions/electrons. Neutrals source is provided by deuterium fueling by gas puff $\Gamma_D = 1 \cdot 10^{21}$ part./s and recycling on carbon wall with reflection coefficient R=1 for main plasma and R = 0.1 for C ions, if present. Two main cases are considered: **STD** "standard" case with two pumping surfaces situated at the entrances of the subdivertor volume (Fig.1A) and **SUBD** "subdivertor" case which mesh incorporates also the subdivertor volume with a pump situated at the surface covering the real cryopump compartment, see Fig. 1B. In this case the gaps between the dome and subdivertor structure are treated as semi-transparent surfaces with reflection coefficients 0.25 and 0.2 for the inner and outer gap, respectively. The albedo of each pumping surface is set to 0.95 (0.1 for C). No seeded impurities were considered. In case of carbon its only source was sputtering described by the Bohdansky formula [3]. For all cases the transport coefficients profile depicted in Fig. 1C was used,

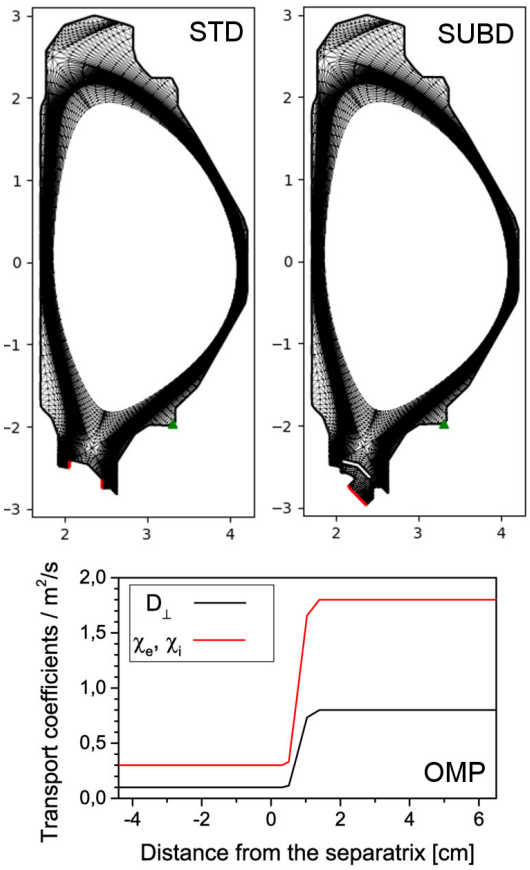

Figure 1: *The meshes used: (STD) with two pumping surfaces, (SUBD) with subdivertor structure and one pumping surface. The position of pumps is marked by red line. D fuelling valve position is marked by ▲. Outer midplane profiles of particle radial diffusion coefficient* $D_\perp$ *and electron and ion heat radial conductivities* χ_e, χ_i, *respectively, are presented below (OMP).*

permanent address: IFPiLM, ul. Hery 23, 01-497 Warszawa, Poland; email: *krzysztof.galazka@ifpilm.pl*

based on previous results [4]. The profiles are expanded over the whole volume according to ψ-map.

Outer midplane profiles Fig. 2 presents the comparison of the electron density n_e and temperature T_e profiles at the outer midplane (OMP) for the case with P_{aux}=15MW. Only a small difference between n_e^{sep} values in the two pure D cases is visible, both reach the value of about $3.6 \cdot 10^{21}$ m^{-3}. For the cases with C (dashed lines) this value lowers to $\sim 3.0 \cdot 10^{19}$ m^{-3}. Both values are higher than the value predicted for the scenario #2 $\leq 2.5 \cdot 10^{19} s^{-1}$ [5]. The table in the figure reports the OMP n_e decay length, resulting mainly from the assumed transport profile. The electron temperature at the separatrix is around 115eV for both geometries, regardless of C impurity presence.

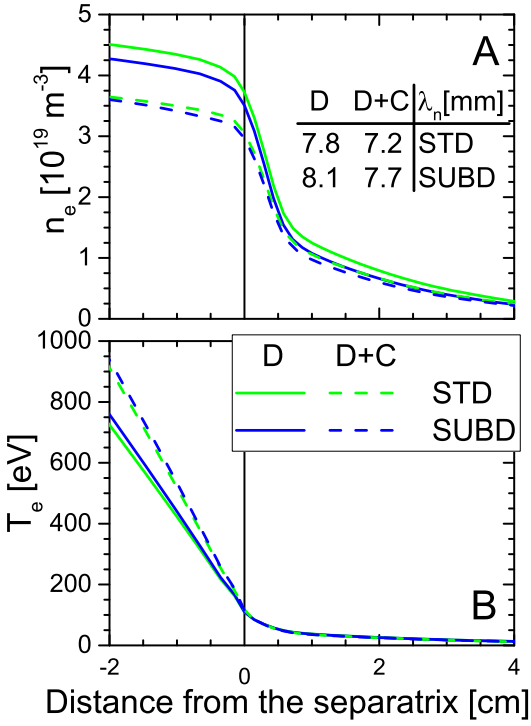

Figure 2: *The OMP n_e profiles for all configurations at P_{aux}=15 MW (A) and the corresponding electron temperature profiles (B).*

Auxiliary heating power scan The results of P_{aux} scan are presented in Fig. 3A and B for the case without and with C impurity, respectively. Increasing P_{aux} gives a major rise to n_e, exceeding the nominal average electron density in the core $\langle n_e \rangle$=5.6$\cdot 10^{19}$m^{-3} for both STD and SUBD cases already at P_{aux}=20 MW, step-wisely moving from scenario #2 to #3 [5]. It is worth noting that the Greenwald density limit n_{GW}=13$\cdot 10^{19}$m^{-3} is still higher than the highest value achieved $n_e \approx 8 \cdot 10^{19}$m^{-3} for the 30MW STD case. Reason for such a big increase lies in a strong increase in the plasma sources (situated mainly in the inner and outer divertor volume). In terms of total values it increases linearly with P_{aux} in the range $[1.5-3.6] \cdot 10^{24}$s^{-1}, whereas for the cases with C the range is $[0.9-1.5] \cdot 10^{24}$s^{-1}. Those are only the plasma sources, the global particle throughput is the same in all cases as the core boundary S_i and Γ_D are not changed. Increased sources lead to larger total amount of particles in the system and explain the lower n_e^{sep} values for the cases with C impurity: from $\sim 3.0 \cdot 10^{19}$ m^{-3} to $\sim 4.2 \cdot 10^{19}$ m^{-3}. In cases with C sputtering increases with P_{aux} leading to an increase of carbon concentration at the OMP n_C^{sep} from 5.5-6.2% for P_{aux} = 15 MW to 9.6-10.3% for the P_{aux}=30 MW case. The average C concentration on the level of 8% was reported previously for COREDIV simulations for a similar n_e^{sep}, but for even higher $P_{aux} \approx 35$ MW [6]. The n_C profiles for the highest P_{aux} cases are somewhat peaked most probably due to not complete convergence. But since C is completely ionized in this region its presence only increases the effective charge. It also should be noted that no pinch was used in the simulations, it can be introduced in the future to account for impurity flushing mechanisms like ELM-s.

In the inset of Fig. 3B the volume integrals of C radiation P_{RAD}^C are presented by the specific region of tokamak chamber. One can see that the largest part of P_{RAD}^C is produced in the outer divertor volume. The inner divertor is about 50% less effective in terms of radiative power dissipation. There is also a non-negligible part of the radiation in the private flux region below the X-point. For all cases P_{RAD}^C states about 1/4 of the P_{aux}. For the P_{aux}=15 MW cases D radiation losses are on the level of 0.7MW.

This results in total amount of heat delivered to both divertor targets at the level of 11 MW.

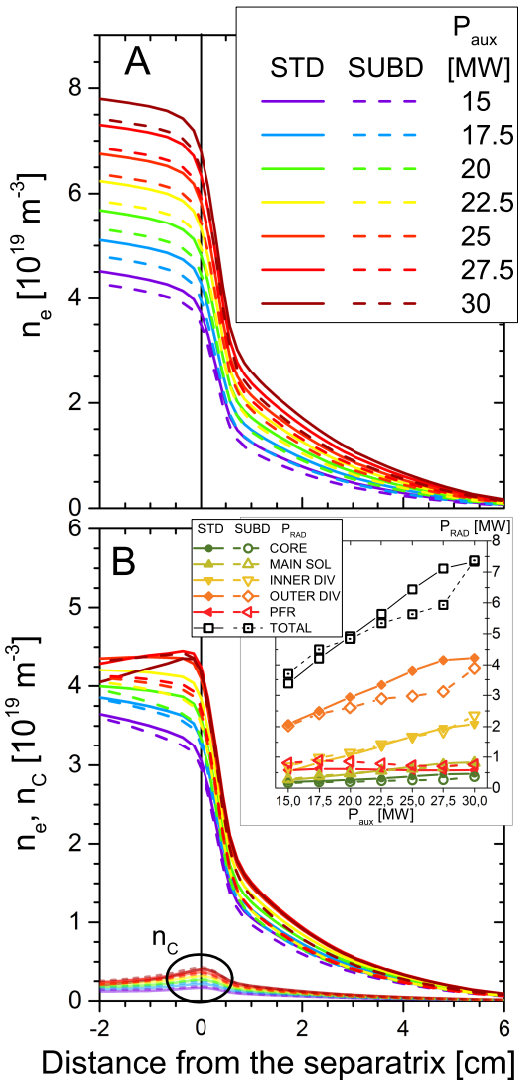

Figure 3: *The OMP n_e profiles for both geometries in P_{aux} scan: (A) presents the results for pure D plasma and (B) with C impurity. In this case also total C concentration profile is presented. The inset: C radiation power split into regions: CORE - confined plasma, MAIN SOL - main chamber SOL, INNER DIV/OUTER DIV - inner/outer divertor volume, PFR - private flux region.*

Conditions at the target plates The case with P_{aux}=15 MW was selected as the most interesting to further investigate in detail. It can be interpreted either as a case with very limited heating power and no additional impurities or a case with substantial energy dissipation in the core plasma by mid/high-Z impurity radiation.

Fig. 4 presents the set of parameters describing the conditions at the targets for the P_{aux}=15 MW case. One can observe that the inner target exhibits lower T_e and higher n_e causing different heat load on both targets [7, 9]. The flattened T_e profiles indicate high density (conduction-limited) regime of operation [8]. For the outer target the peak heat load Q_{TOT}^{MAX} exceeds the steady-state operational limit (10 MWm^{-2}) already at this relatively low heating power for all investigated cases [5]. This findings are in agreement with previous modeling [4] and similar conclusion follows: for a safe scenario operation an additional power dissipation mechanism is required, for instance by a seeded mid-Z impurity.

For the cases with C the peak heat load on the targets is visibly lower for the SUBD case, especially for the outer target. It should be mentioned that among the investigated cases neutrals deliver at maximum $\sim$ 2.6 MWm^{-2}, which is a remarkable fraction (about 20%) of the local Q_{TOT}. For the rest of the chamber wall the highest heat load is on the corner of the dome close to the inner target. In the cases with C it receives about 0.1 MWm^{-2}. This is well below the operational limit for this element (1.0 MWm^{-2} specified in the JT-60SA Plant Integration Document). Even for the highest P_{aux} case its heat load never exceeds 0.5 MWm^{-2}. The last observation is that despite different neutrals distribution in the OT region (compare Fig.4G and H) the final results seem not to be affected by different geometry. Important is what are the conditions at the strike points, and these converge to a similar working point, regardless how the neutrals fill up the available space. However, a presence of the subdivertor volume might have a bigger influence while modeling detachment.

Conclusions A power scan was performed for the fully inductive scenario #2 of JT-60SA in the range of $[15, 30]$ MW. In the pure-D case with increasing P_{aux} the n_e^{sep} increases and $\langle n_e \rangle$ exceeds the nominal scenario value due to increase of plasma source at the targets. In the cases with C this increase is less pronounced due lower power reaching targets in presence of C radiation. For those

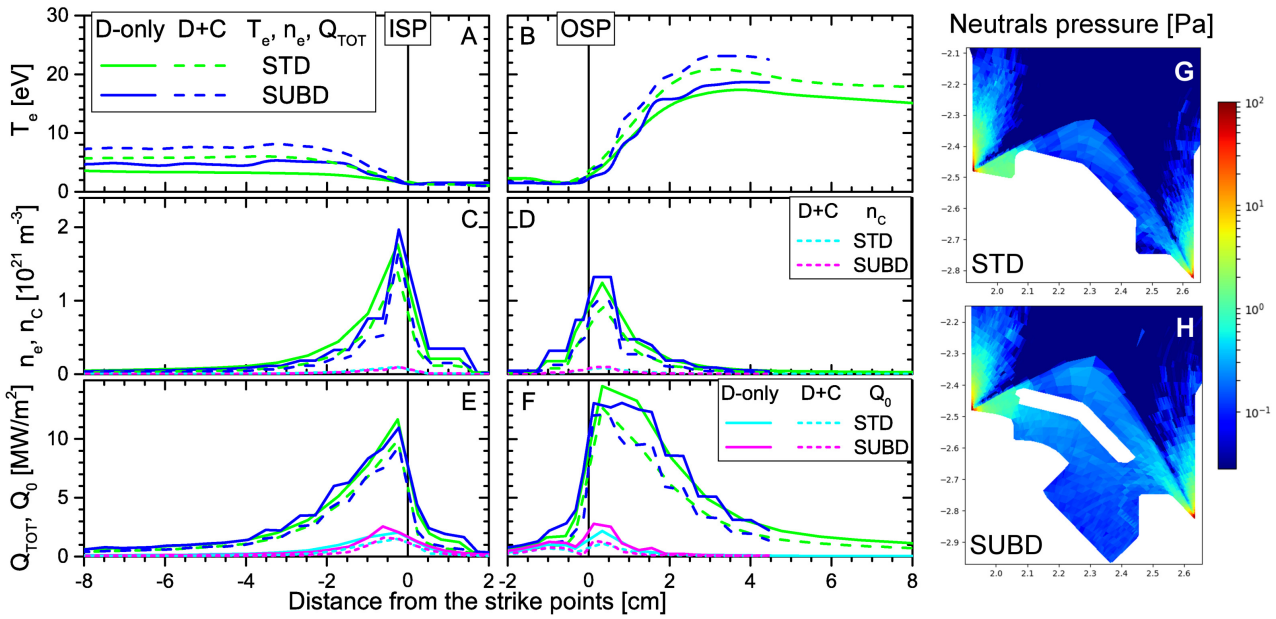

Figure 4: *Comparison of the inner and outer target profiles for the P_{aux}=15 MW case: (A, B) - electron temperature, (C, D) - electron density and carbon density, (E, F) - total heat load Q_{TOT} and the contribution of neutral particles Q_0. ISP and OSP - inner and outer strike point, respectively. (G, H) - the neutral pressure in the divertor and subdivertor volume for the cases with C.*

C concentrations between 5.5% and 10.3% are observed. Even for the lowest P_{aux}=15 MW the heat load at the outer target exceeds the steady-state operational limit of 10 MWm^{-2} indicating a need of an additional power dissipation mechanism in the SOL/pedestal. For the investigated working point the results for STD and SUBD geometries do not differ significantly (1MW corrections to $P_{\mathrm{RAD}}^{\mathrm{C}}$ at higher P_{aux} in the outer target volume).

References

[1] H. Bufferand *et al.*, Nucl. Fusion **61**, 116052 (2021)

[2] N. Hayashi *et al.*, Proc. 26th IAEA Fusion Energy Conf., (2016)

[3] J. Bohdansky, Nucl. Instr. and Meth. B **2**, 587 (1984)

[4] L. Balbinot *et al.*, to be submitted to Nucl. Mat and Energy

[5] JT-60SA Research Plan *ver. 4.0* (2018)

[6] R. Zagórski *et al.*, Nucl. Fusion **56**, 016018 (2016)

[7] W. Fundamentski *et al.*, Journal of Nucl Materials **313-316**, 787 (2003)

[8] P. C. Stangeby, *The plasma boundary of magnetic fusion devices*, Inst. of Phys. Publ. Bristol and Philadelph (2000)

[9] A. Loarte *et al.*, ITPA Scrape-off Layer, and Divertor Physics Topical Group., Nucl. Fusion, **47**, 203 (2007)